3DAP Study on Carbon Segregation Behavior During Cryogenic Treatment of High-Carbon High-Alloy Steel (Postprint)

Authors: Xie Chen, Wu Xiaochun, Min Na, Shen Yunliang

Date: 2016-11-04T00:00:00+00:00

Abstract

High-carbon high-alloy steel SDC99 was austenitized at 1030 ℃ for 30 min, followed by oil quenching, cryogenic treatment in liquid nitrogen at -196 ℃ for 8 h, and tempering at 210 ℃ for 2 h. The spatial distribution of carbon atoms in the as-quenched, cryogenically-treated, and tempered states was analyzed using three-dimensional atom probe (3DAP) technology; XRD was used to investigate the changes in martensite axial ratio and carbon content in martensite under the three heat treatment conditions; SEM was employed for in-situ observation of carbide morphology before and after cryogenic treatment. The results indicate that no carbides precipitated before or after cryogenic treatment, and carbon atoms segregated to martensite twin boundaries during the cryogenic treatment process, forming segregation zones with a thickness of 5–10 nm. During low-temperature tempering at 210 ℃, carbon further segregated to form carbon-rich phases or precipitated as M23C6-type carbides with alloy atoms.

Full Text

Carbon Segregation Behavior of High-Carbon High-Alloy Steel During Deep Cryogenic Treatment Using 3DAP

XIE Chen, WU Xiaochun, MIN Na, SHEN Yunliang
School of Materials Science and Engineering, Shanghai University, Shanghai 200072

Correspondent: WU Xiaochun, professor, E-mail: xcwu@staff.shu.edu.cn
Supported by National Natural Science Foundation of China (No. 51171104)

Manuscript received 2014-08-02, in revised form 2015-01-06

Abstract

Deep cryogenic treatment (DCT) is a supplement to conventional heat treatment, which typically involves cooling materials to liquid nitrogen temperature (approximately -196°C) for a specified soaking period before reheating to room temperature. Numerous pioneering studies have demonstrated that DCT can significantly improve the hardness and wear resistance of high-carbon high-alloy steels, leading to widespread application in die steels, cutting tools, carburizing steels, and barrels. The enhancement of mechanical properties through DCT has been attributed to the transformation of retained austenite to martensite, the fine dispersion of nanoscale carbide precipitates, and the relief of residual stresses. However, direct evidence for nanoscale carbide precipitation remains scarce, and interpretations of carbon segregation behavior during DCT are still unconvincing.

In this study, the high-carbon high-alloy steel SDC99 was austenitized at 1030°C for 30 minutes, oil-quenched, subjected to deep cryogenic treatment in liquid nitrogen at -196°C for 8 hours, and finally tempered at 210°C for 2 hours. The spatial distribution of carbon atoms and alloy element concentrations in quenched, DCT-treated, and tempered samples was analyzed using three-dimensional atom probe (3DAP). Additionally, X-ray diffraction (XRD) was employed to investigate changes in the martensite axial ratio and carbon content under the three heat treatment conditions, while scanning electron microscopy (SEM) was used for in situ observation of carbide morphology before and after DCT.

The results indicate that after quenching from 1030°C to room temperature, the volume fraction of retained austenite in SDC99 was approximately 21.1%. This soft and unstable retained austenite readily transforms to martensite at lower temperatures, while carbon atoms exhibit slight segregation due to self-tempering. However, other alloy atoms did not co-segregate with carbon atoms. After quenching and subsequent cooling in liquid nitrogen for 8 hours, the retained austenite volume fraction decreased to 7.4%, and carbon atoms segregated along martensite twin boundaries, forming segregation zones with a thickness of 5-10 nm. No carbide precipitation occurred after DCT. Furthermore, carbon atoms segregated again during reheating from -196°C to room temperature. After tempering at 210°C for 2 hours, the retained austenite volume fraction was approximately 5.4%. Both carbon and alloy atoms segregated during tempering at 210°C. With increasing tempering time, carbon segregation intensified, resulting in either a carbon-rich phase or the formation of $M_{23}C_6$-type carbides in combination with other alloy elements. This represents one of the primary mechanisms for the improved wear resistance of tool steels.

KEY WORDS high-carbon high-alloy steel, deep cryogenic treatment (DCT), carbon segregation, carbide morphology, 3DAP

1. Introduction

Deep cryogenic treatment (DCT) is a heat treatment process that improves hardness, wear resistance, and dimensional stability by holding workpieces in cryogenic environments below -130°C (typically using liquid nitrogen). This process significantly enhances the wear resistance of high-carbon high-alloy steels such as tool steels, bearing steels, carburizing steels, and high-speed steels. However, the underlying microscopic mechanisms remain unclear and have become a focal point of research worldwide [1].

Understanding the effect of the cryogenic process on carbide precipitation is crucial for investigating the mechanisms behind improved wear performance. Huang et al. [2] statistically analyzed the carbide size distribution in M2 high-speed steel before and after DCT, finding that the average carbide diameter decreased from 0.9 m to 0.6 m. Das et al. [3] examined the size and distribution of carbides in D2 steel after DCT using scanning electron microscopy. Meng et al. [4] observed carbides in Fe-12Cr-Mo-V-1.4C after DCT using transmission electron microscopy and proposed that the expansion and contraction of the martensite lattice promoted the precipitation of fine -carbides. Li et al. [5-8] investigated the effects of DCT on Snoek and SKK peaks in cold work die steel using internal friction methods, suggesting that DCT enhances the interaction between carbon atoms and dislocations. Current research generally supports the view that DCT promotes nanoscale carbide precipitation. However, the diffusion capacity of carbon atoms decreases exponentially with temperature, and it is widely accepted that carbon atoms cannot move below -100°C [9], which cannot explain carbide precipitation after DCT. Moreover, the aforementioned detection methods lack the precision and directness required for analyzing nanoscale carbides precipitated during the cryogenic process, necessitating more sophisticated equipment for direct observation of carbon segregation during DCT.

Three-dimensional atom probe (3DAP) can provide the distribution of different chemical elements in a sample at the nanoscale and represents one of the most microscopically precise analytical techniques available. Zhu et al. [10] studied carbon segregation during low-temperature tempering of Fe-Ni-C alloys and AISI 4340 (40CrNi2Mo) alloy steel, presenting for the first time the three-dimensional structure of carbon-rich zones and microscale defects. Wilde et al. [11] used 3DAP to investigate Cottrell atmospheres in three low-carbon steel samples with different carbon contents after quenching at 1000-1100°C and aging at room temperature. Liu et al. [12-14] studied the nucleation, growth, and coarsening processes of alloy carbides in tempered martensite. These studies demonstrate that 3DAP can directly reveal the microstructure of nanoscale precipitates. However, 3DAP characterization of carbon segregation behavior during DCT of high-carbon high-alloy steels has not been reported. Therefore, this work combines X-ray diffraction (XRD) and scanning electron microscopy (SEM) with 3DAP to investigate the spatial distribution of carbon atoms in a high-carbon high-alloy steel during quenching, DCT, and tempering, explor-

ing microstructural evolution and the processes of carbon diffusion, segregation, and precipitation to elucidate the mechanisms of carbon segregation and carbide precipitation during DCT.

2. Experimental

The study employed a high-strength, high-toughness cold work die steel SDC99 developed by our research group, with a chemical composition (mass fraction, %) of: C 0.83, Si 0.57, Mn 0.51, Cr 9.37, Mo 1.46, V 0.28, Fe balance. The atomic fractions were: C 3.73, Si 1.01, Mn 0.50, Cr 9.72, Mo 0.82, V 0.30, Fe balance. Three heat treatment processes were applied as shown in Table 1. Annealed samples were austenitized at 1030°C for 30 minutes and oil-quenched. Some quenched samples were retained, while others were held in a liquid nitrogen tank for 8 hours before removal. Some DCT-treated samples were retained, while the remainder were tempered at 210°C.

Samples measuring 10 mm × 10 mm × 10 mm were cut from the three heat-treated specimens using wire electrical discharge machining. Rockwell hardness was measured using an HD 9-45 hardness tester to characterize changes in macroscopic properties. Phase analysis was performed using a D/max-2200 X-ray diffractometer (XRD) with a rotating Cu target (wavelength $\lambda = 1.5418 \times 10^{-10}$ m), scanning angle range of 30°-110°, and scanning speed of 1°/min. The volume fraction of retained austenite was calculated using the following formula [15]:

$$V_\gamma = \frac{I_\gamma R_\alpha}{I_\alpha R_\gamma + I_\gamma R_\alpha} \times (1 - V_C)$$

where I_γ and I_α are the integrated intensities of austenite and martensite diffraction lines, respectively; R_γ and R_α are the structure factors of austenite and martensite, respectively; and V_C is the volume fraction of carbides. Due to the small volume fraction of carbides, this term was neglected in calculations.

Microhardness indentations were made using an MH-3 Vickers hardness tester. In situ observation of microstructural morphology before and after DCT was performed using a Supra 40 field-emission scanning electron microscope (SEM) with energy-dispersive spectroscopy (EDS). The spatial distribution of elements in quenched, DCT-treated, and tempered samples was analyzed using a LEAP 4000X HR 3DAP. The three heat-treated samples were cut into needle-shaped specimens measuring 0.5 mm × 0.5 mm × 55 mm using wire electrical discharge machining, and the required needle-tip samples were prepared using a two-step electropolishing method [16]. The 3DAP data were post-processed using Posap software. JMat Pro® thermodynamic software was used to calculate the equilibrium carbide types and quantities.

2.1 Hardness and Phase Composition

The hardness values of high-carbon high-alloy steel SDC99 after quenching at 1030°C, holding at -196°C for 8 hours, and tempering at 210°C for 2 hours are presented in Table 1. The as-quenched hardness of SDC99 was 62 HRC, which increased to 64 HRC after DCT—a 2 HRC improvement attributed to the transformation of retained austenite to martensite. After tempering at 210°C, the hardness slightly decreased to 63 HRC, a 1 HRC reduction from the DCT state. During low-temperature tempering, carbides precipitate from martensite, reducing the carbon content of the matrix and resulting in slightly lower hardness compared to the DCT state.

Figure 1 [FIGURE:1] shows the XRD patterns of the three samples after quenching, DCT, and tempering. The volume fraction of retained austenite was calculated using diffraction lines from martensite (200) and (211) planes and austenite (200) , (220) , and (311) planes [17], with results summarized in Table 1. The as-quenched microstructure of SDC99 consisted primarily of cryptocrystalline martensite, retained austenite, and undissolved carbides, with a retained austenite volume fraction of 21.1%. After DCT, the retained austenite volume fraction decreased to 7.4% (a 13.7% reduction), explaining the increased hardness. In the tempered sample, the retained austenite content was 5.4%, showing only a modest decrease from the DCT state. This is because the retained austenite that did not transform during DCT was highly stable and under a state of equiaxial compressive stress, making further transformation difficult during subsequent tempering. While excessive retained austenite in high-alloy steels reduces material strength, retaining a certain amount can improve toughness and wear resistance [18,19]. Therefore, the performance of SDC99 steel after DCT and tempering is superior to conventional heat treatment [20].

In Figure 1, the diffraction intensities of (200) , (220) , and (311) planes decreased significantly after DCT and further diminished after tempering, while the intensities of (200) and (211) planes continuously increased. After DCT and tempering, the martensite diffraction peaks gradually narrowed and shifted, indicating changes in carbon content within martensite [21].

To further analyze carbon segregation and carbide precipitation behavior, the martensite axial ratio (c/a) and carbon content were calculated using empirical formulas [22]. Martensite has a body-centered tetragonal structure with interplanar spacings given by:

$$d_{(hkl)} = \frac{a}{\sqrt{h^2+k^2+l^2}} \cdot \frac{1}{\sqrt{1+\left(\frac{c^2}{a^2}-1\right)\cdot\frac{l^2}{h^2+k^2+l^2}}}$$

Using the (200) and (112) planes for calculation:

$$\frac{d_{(200)}}{d_{(112)}} = \frac{\sqrt{6}}{2\sqrt{1+\left(\frac{c^2}{a^2}-1\right)\cdot\frac{1}{6}}}$$

According to Kurdjumov [22], the relationship is:

$$\frac{c}{a} = 1 + 0.116 \times p$$

where h, k, l are Miller indices; $d_{(hkl)}$ is the interplanar spacing of the (hkl) plane; a and c are the lattice constants of martensite; α_0 is the lattice constant of α-Fe; and p is the carbon content in martensite.

The calculated c/a ratios after quenching, DCT, and tempering were 1.0289, 1.0278, and 1.0267, respectively, with corresponding carbon mass fractions in martensite of 0.64%, 0.61%, and 0.59%. These results show that DCT reduces martensite tetragonality and lattice distortion, decreasing carbon content compared to the quenched state. During DCT, the martensite lattice contracts, placing supersaturated carbon atoms under significant stress within the lattice and creating a thermodynamically unstable state that increases the tendency for diffusion to defects or carbide precipitation. However, the DCT holding temperature is extremely low (-196°C), and carbon atoms are generally considered immobile below -100°C. Therefore, the plastic deformation induced by martensitic transformation during cryogenic treatment increases dislocation density, and dislocation glide captures and transports carbon atoms [23]. After tempering, the matrix carbon content further decreases, indicating that carbon atoms may continue to segregate to defects such as dislocations and twin boundaries or form carbide precipitates during low-temperature tempering.

2.2 Microstructural Morphology

Figure 2 [FIGURE:2] presents SEM images of SDC99 steel after quenching and DCT. To investigate whether carbides precipitate during DCT, SEM images were taken in situ at the locations shown in Figures 2a and 2c after cryogenic treatment (Figures 2b and 2d). Figures 2a and 2c reveal carbides approximately 0.2-1.0 m in size distributed on the quenched martensite matrix. After DCT (Figures 2b and 2d), some fine carbides had detached, but no new nanoscale carbide particles were observed, confirming that significant carbide precipitation does not occur during DCT. Carbide precipitation should therefore take place during the tempering process [24].

2.3 3DAP Analysis

Figure 3 [FIGURE:3] shows the spatial distributions of major alloying elements (C, Cr, Mo, and V) in as-quenched SDC99 steel obtained by 3DAP. The atomic fractions of C, Cr, Mo, V, Si, and Mn in the sampled region were 1.63%, 5.04%,

0.69%, 0.13%, 1.13%, and 0.29%, respectively, indicating that the analyzed region was primarily quenched martensite with supersaturated carbon. The figure shows that major alloying elements Cr, Mo, and V were uniformly distributed, while carbon exhibited local segregation. This occurs because SDC99 has high alloy content and a martensite start temperature (M) of 220°C [25], which is above room temperature, causing self-tempering after quenching [26]. Carbon atoms undergo short-range diffusion and segregate to defects such as dislocations, while Cr cannot form alloy carbide precipitates. Consequently, alloying elements were uniformly distributed in the as-quenched sample, with only slight carbon segregation observed.

To further investigate carbon distribution and concentration variations, three-dimensional atom reconstruction of carbon atoms from Figure 3 was performed, yielding isoconcentration surface maps at 4%, 4.5%, and 5% carbon, as shown in Figure 4 [FIGURE:4]. Carbon distribution was relatively uniform, with only localized regions exceeding 4% carbon content. This is attributed to the fact that during the pre-quenching holding period, carbon and other alloying elements were fully dissolved in the matrix. The rapid cooling rate during quenching, necessary to obtain martensite, maintained carbon and alloying elements in their high-temperature supersaturated state. However, high-carbon high-alloy steels retain some retained austenite after quenching to room temperature, so regions with higher carbon concentrations may correspond to retained austenite phases.

Figure 5 [FIGURE:5] displays the spatial distributions of various elements in SDC99 steel after quenching and DCT at -196°C for 8 hours. After DCT, carbon exhibited significant segregation, with trace vanadium co-segregating in carbon-rich regions, while Cr and Mo did not form notable segregation zones. Vanadium is a strong carbide-forming element with a high chemical affinity for carbon, making it prone to co-segregation with carbon. In contrast, Cr and Mo are moderate carbide-forming elements with lower binding capacity to carbon.

During DCT, retained austenite transforms to martensite under the combined effects of temperature and stress. Carbon segregation may result from two mechanisms: (1) plastic deformation induced by martensitic transformation during cryogenic treatment increases dislocation density [27], and dislocation glide transports carbon atoms [23]; and (2) under intense stress, retained austenite transforms to twinned martensite [15,28], and carbon atoms segregate at twin/matrix interfaces during reheating to room temperature. To further examine these carbon segregation zones, a 40 nm-long region was analyzed for carbon content, as shown in Figure 6

. The average carbon content in this region was approximately 4%, far lower than that of cementite (25%) or -carbide (25-33%), and the carbon distribution did not form typical carbide morphologies. Therefore, the likely phases or microstructures in this region are retained austenite and twinned martensite, or simply carbon segregation at interfaces or defects.

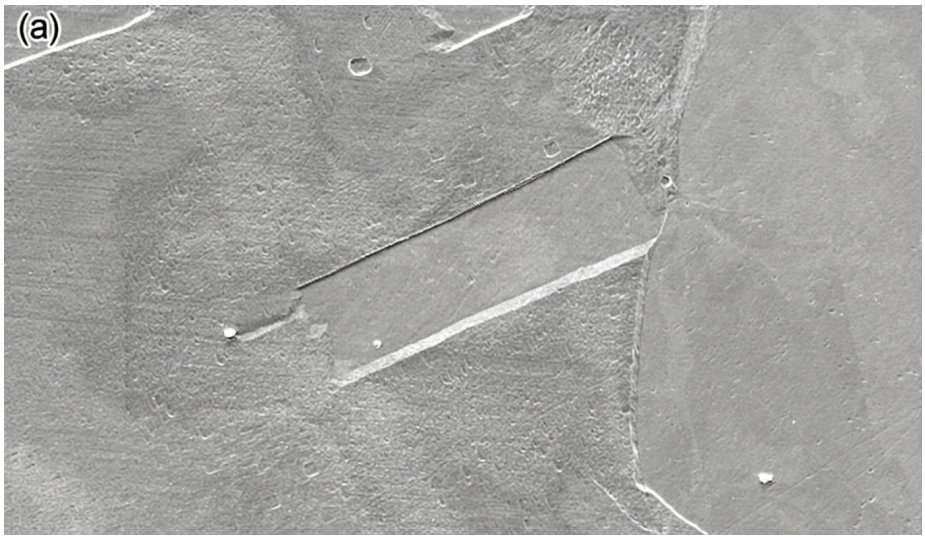

Figure 1: Figure 6

Three-dimensional atom reconstruction of the sampled region was performed to analyze isoconcentration surfaces at 4%, 4.5%, and 5% carbon, with results shown in Figure 7 [FIGURE:7]. Carbon atoms segregated in parallel plate-like configurations, with these segregation zones spaced approximately 5-10 nm apart. Generally, the carbon content of bulk retained austenite ranges from 2.5% to 5.61%. The volume fraction of these segregation zones accounted for 40-50% of the entire microstructure. Since SDC99 steel contained only 7.4% retained austenite after DCT, these regions cannot be retained austenite phases. Gavriljuk et al. [23] used Mössbauer spectroscopy to study cryogenic treatment and concluded that plastic deformation from low-temperature martensitic transformation drives carbon atoms to dislocations. However, the plate-like parallel segregation shown in Figure 7 does not match the morphology of dislocation segregation.

Considering that retained austenite transforms to martensite during DCT, the newly formed martensite has high carbon content and, due to limited carbon diffusion at low temperatures, develops a twinned substructure that provides abundant interfaces for carbon segregation. Simultaneously, the martensite lattice contracts at cryogenic temperatures, placing supersaturated carbon atoms under significant compressive stress within the lattice. Under prolonged stress, carbon atoms readily segregate at twin boundaries. These carbon-rich segregation zones can be understood as pre-precipitation stages before carbide formation, analogous to Guinier-Preston (G.P.) zones formed during aging of Al-Cu alloys.

Figure 8 [FIGURE:8] shows the spatial distribution of carbon atoms and al-

loy element concentrations in different regions of SDC99 steel after DCT and tempering at 210°C for 2 hours. Two types of carbon segregation zones were observed: (1) multiple plate-like carbon-rich zones in the lower portion of the sample (Area I), and (2) an alloy carbide region approximately 60 nm × 60 nm × 20 nm at the top (Area II). Concentration analysis of Area I (Figure 8b) revealed a maximum carbon concentration of 14%, forming a carbon-rich phase approximately 10 nm thick that resulted from further segregation of carbon segregated during DCT. The chromium content in this carbon-rich region was similar to the matrix, but reached 14% at the carbon-rich region/matrix interface. The non-carbide-forming element silicon segregated at this interface, hindering growth of the carbon-rich phase. Area II formed alloy carbides, with concentration profiles shown in Figure 8c. These carbides were rich in Cr and Mo, and stoichiometric calculations identified them as $M_{23}C_6$-type carbides, consistent with JMatPro calculations showing that $M_{23}C_6$ carbides readily precipitate during low-temperature tempering (Figure 9 [FIGURE:9]).

The martensite finish temperature (M_f) of high-carbon high-alloy steel SDC99 is below room temperature at approximately -30°C [29]. Therefore, the as-quenched microstructure consists of quenched martensite, retained austenite, and a small amount of eutectic carbides. Quenched martensite is a supersaturated solid solution of carbon and alloying elements in α-Fe. 3DAP observations revealed relatively uniform carbon distribution in the as-quenched state (average carbon content of 1.63 at%), with only localized regions showing higher carbon concentrations (>4 at%), likely corresponding to retained austenite (17.6 vol%). Retained austenite is a metastable phase with low hardness that readily transforms to harder martensite under increased stress and decreased temperature.

When quenched SDC99 samples were cryogenically treated at -196°C, approximately 9.9% of retained austenite transformed to martensite due to temperature reduction and increased stress [15], increasing sample hardness. However, DCT could not completely eliminate retained austenite, with 7.7% remaining untransformed. Retained austenite has a face-centered cubic structure with low stacking fault energy. The macroscopic contraction caused by rapid cooling during DCT induces slip in stacking planes, resulting in a twinned substructure in the newly formed martensite [28] that provides sites for supersaturated carbon segregation. It should be noted that carbon diffusion capacity decreases exponentially with temperature, and carbon atoms cannot be thermally activated for diffusion at cryogenic temperatures. However, plastic deformation during martensitic transformation introduces numerous dislocations [23], and dislocation motion can capture and transport carbon atoms that are “frozen” at low temperatures. During reheating from cryogenic temperature to room temperature, when the temperature exceeds -50°C, carbon atoms gain sufficient thermal activation for diffusion along grain boundaries. However, diffusion remains difficult, and carbon atoms preferentially segregate along “short-circuit paths” such as twin boundaries or dislocations, providing effective nucleation sites for carbide precipitation and growth during tempering. The 3DAP results show segregation zones approximately 5-10 nm in size with carbon concentra-

tions near 4 at%. At cryogenic or room temperature, alloy atoms such as Fe, Cr, Mo, and V cannot diffuse, preventing carbide formation.

During tempering at 210°C, carbon atom mobility increases with temperature, and alloy atoms such as Cr and Mo also gain sufficient thermal activation for diffusion. This occurs because substantial retained austenite transforms to twinned martensite during DCT [15]. However, alloy element diffusion is difficult at low temperatures, and only carbon atoms can diffuse upon returning to room temperature, preventing alloy carbide precipitation. Nevertheless, twins and dislocations formed during DCT provide effective nucleation sites for carbides. During tempering at 210°C, carbon atoms segregated during DCT continue to enrich, forming plate-like carbon-rich phases approximately 10 nm thick with carbon concentrations up to 14 at%, while Cr and other elements develop diffusion capacity. Simultaneously, carbon combines with Fe, Cr, Mo, and V to form stoichiometric $M_{23}C_6$-type carbides. The alloy carbides precipitated at this temperature are extremely fine and dispersed throughout the matrix, enhancing the wear resistance of high-carbon high-alloy steels [30]. Additionally, 5.2% retained austenite remained in the matrix after low-temperature tempering. This retained austenite, which survived both DCT and tempering, is a highly stable structure that typically exists as thin films around martensite laths, relieving stress and improving material toughness, which benefits wear resistance.

3. Conclusions

1. After quenching high-carbon high-alloy steel SDC99 from 1030°C to room temperature, the retained austenite volume fraction was 21.1%. Due to self-tempering, carbon atoms exhibited slight segregation.
2. After quenching and DCT at -196°C for 8 hours, the retained austenite partially transformed to martensite, decreasing its volume fraction to 7.4%. Carbon atoms segregated at the boundaries of newly formed martensite grains and further segregated during reheating from cryogenic temperature to room temperature, forming parallel plate-like segregation zones 5-10 nm thick without precipitating as carbides.
3. After quenching, DCT at -196°C for 8 hours, and tempering at 210°C for 2 hours, the retained austenite volume fraction was 5.4%. Carbon atoms segregated at the boundaries of newly formed twinned martensite during DCT either further enriched to form carbon-rich phases approximately 10 nm thick or combined with Cr and Mo to precipitate as $M_{23}C_6$ carbides. These nanoscale carbides dispersed in the matrix represent the key reason for the significantly improved wear resistance of high-carbon high-alloy steels after DCT.

Acknowledgments: The authors thank Associate Professor Li Junwan from the School of Materials Science and Engineering at Shanghai University for valuable suggestions on manuscript revision.

References

[1] Baldissera P, Delprete C. Open Mech Eng J, 2008; 2(8): 1
[2] Huang J Y, Zhu Y T, Liao X Z, Beyerlein I J, Bourke M A, Mitchell T E. Mater Sci Eng, 2003; A339: 241
[3] Das D, Dutta A K, Toppo V, Ray K K. Mater Manuf Processes, 2007; 22: 47
[4] Meng F, Tagashira K, Azuma R, Sohma H. ISIJ Int, 1994; 34: 205
[5] Li S H, Deng L H, Wu X C, Wang H B, Min Y A. Mater Sci Eng, 2010; A527: 6899
[6] Li S H, Deng L H, Wu X C, Wang H B, Min Y A, Min N. Mater Sci Eng, 2010; A527: 7950
[7] Li S H, Min N, Deng L H, Wu X C, Min Y A, Wang H B. Mater Sci Eng, 2011; A528: 1247
[8] Li S H, Min N, Li J W, Wu X C, Li C H, Tang L L. Mater Sci Eng, 2013; A575: 51
[9] Tyshchenko A I, Theisen W, Oppenkowski A, Siebert S, Razumov O N, Skoblik A P. Mater Sci Eng, 2010; A527: 7027
[10] Zhu C, Cerezo A, Smith G D W. Ultramicroscopy, 2009; 109: 545
[11] Wilde J, Cerezo A, Smith G D W. Scr Mater, 2000; 43: 39
[12] Liu Q D, Liu W Q, Wang Z M, Zhou B X. Acta Metall Sin, 2009; 45: 1281
[13] Liu Q D, Peng J C, Liu W Q, Zhou B X. Acta Metall Sin, 2009; 45: 1288
[14] Liu Q D, Chu Y L, Peng J C, Liu W Q, Zhou B X. Acta Metall Sin, 2009; 45: 1297
[15] Matteo V, Karen P, Marcel A J S. Acta Mater, 2014; 65: 383
[16] Liu Q D, Liu W Q, Wang Z M, Zhou B X. Acta Metall Sin, 2008; 44: 786
[17] Xie Z J, Ren Y Q, Zhou W H, Yang J R, Shang C J, Misra R D K. Mater Sci Eng, 2014; 603: 69
[18] Clarke A J, Speer J G, Miller M K, Hackenberg R E, Edmonds D V, Matlock D K, Rizzo F C, Clarke K D, Moor E De. Acta Mater, 2008; 56: 16
[19] Gao G H, Zhang H, Gui X L, Luo P, Tan Z L, Bai B Z. Acta Mater, 2014; 76: 425
[20] Li S H, Xie Y Z, Wu X C. Cryogenics, 2010; 50: 89
[21] Duan C Z, Wang M J. J Iron Steel Res, 2008; 20(8): 38
[22] Kurdjumov G V. Metall Trans, 1976; 7A: 999
[23] Gavriljuk V G, Theisen W, Sirosh V V, Polshin E V, Kortmann A K, Mogilny G S, Petrov Y N, Tarusin Y V. Acta Mater, 2013; 61: 1705
[24] Tyshchenko A I, Theisen W, Oppenkowski A, Siebert S, Razumov O N, Skoblik A P, Sirosh V A, Petrov Y N, Gavriljuk V G. Mater Sci Eng, 2010; A527: 7027
[25] Li J W, Tang L L, Li S H, Wu X C. Mater Des, 2013; 47: 653
[26] Liu Q D, Chu Y L, Wang Z M, Liu W Q, Zhou B X. Acta Metall Sin, 2008; 44: 1281
[27] Li S H, Deng L H, Wu X C, Min Y A, Wang H B. Cryogenics, 2010; 50: 754
[28] Li S Y, Liu T Z, Li G. Mater Rev, 2003; 17: 80

[29] Li J W, Feng Y, Tang L L, Wu X C. Mater Lett, 2013; 100: 274
[30] Li S H. PhD Dissertation, Shanghai University, 2011